Finite element simulations of the head–brain responses to the top impacts of a construction helmet: Effects of the neck and body mass

John Z Wu[1], **Christopher S Pan**[1], **Bryan M Wimer**[1], and **Charles L Rosen**[2]

[1]National Institute for Occupational Safety and Health (NIOSH), Morgantown, WV, USA

[2]Department of Neurosurgery, West Virginia University, Morgantown, WV, USA

Abstract

Traumatic brain injuries are among the most common severely disabling injuries in the United States. Construction helmets are considered essential personal protective equipment for reducing traumatic brain injury risks at work sites. In this study, we proposed a practical finite element modeling approach that would be suitable for engineers to optimize construction helmet design. The finite element model includes all essential anatomical structures of a human head (i.e. skin, scalp, skull, cerebrospinal fluid, brain, medulla, spinal cord, cervical vertebrae, and discs) and all major engineering components of a construction helmet (i.e. shell and suspension system). The head finite element model has been calibrated using the experimental data in the literature. It is technically difficult to precisely account for the effects of the neck and body mass on the dynamic responses, because the finite element model does not include the entire human body. An approximation approach has been developed to account for the effects of the neck and body mass on the dynamic responses of the head–brain. Using the proposed model, we have calculated the responses of the head–brain during a top impact when wearing a construction helmet. The proposed modeling approach would provide a tool to improve the helmet design on a biomechanical basis.

Introduction

Traumatic brain injuries (TBIs) are among the most common severely disabling injuries in the United States. During 2002–2006, approximately 1.7 million cases occurred in civilians

annually.[1] A total of 7294 work-related TBI fatalities were identified during 2003–2008, which accounted for 22% of all occupational injury fatalities.[2] Among the leading causes of work-related TBI death, falls and contact with objects/equipment occupied 47%.[2] The work-related TBI fatalities due to fall or contact with objects may potentially be reduced using proper helmets. The finite element (FE) method has been widely used to understand the injury mechanism of TBI.[3] In order for the FE method to generate reliable simulations, the models must include realistic geometries, reliable material properties, and physiological boundary/loading conditions of the biological systems.

Over the last three decades, tremendous progress has been made in the development of FE models in the investigation of injury mechanisms and in the design of head protective systems. The human head–brain modeling has progressed from early models with linear material properties and simplistic geometries[4,5] to the current sophisticated models including nonlinear and time-dependent material properties, realistic geometries, and detailed anatomical structures.[6–8] FE models have been applied in solving practical problems. For example, Patton et al.[9] developed a detailed FE head model to simulate unhelmeted concussion in sport; Tse et al.[10,11] developed subject-specific models to numerically reconstruct accidents to investigate the relations between traumatic facial injuries and brain injuries. Most of these head–brain models are used for frontal impacts and do not include the neck. It is widely believed that the effects of the neck and body mass on the brain responses during short impact intervals (duration less than 7 ms) are negligible;[12,13] however, the effects of the neck and body mass have not been quantified.

Afshari and Rajaari[14] developed FE models to study the protective effectiveness of the helmet during the head–ground impact of a motorcyclist. Teng et al.[15] developed FE models of a bicycle helmet with foam liners and validated their model with impact tests. Although these models included detailed helmet geometries and material properties, they did not include realistic anatomical structures of the human head. Yang and Dai[16] developed FE models to study the ballistic helmet impact; their models included realistic geometries and material properties of the helmet and human head. Their models have been further developed by Long et al.[17] to assess the performance of construction helmets.

The helmets used by construction site workers[18,19] are mainly designed for protection from objects, usually with a larger mass, that are dropped on the top of helmet in a vertical direction.[20] Ballistic helmets are mainly used for the protection from object impact or penetration, where the object has a smaller mass and impacts with the front of the helmet.[16] The head–helmet stiffness in the top impact may be greater than that in the frontal impact, because of the effects of the neck and body mass. Our hypothesis is that the neck and body mass will have effects on the head–brain responses for top impact of a construction helmet. Our goal is to develop a practical FE model that would be suitable for engineers to optimize construction helmet design. The FE model will include all essential anatomical structures of a human head (i.e. skin, scalp, skull, cerebrospinal fluid (CSF), brain, medulla, spinal cord, cervical vertebrae, and discs) and all major engineering components of a construction helmet (i.e. shell and suspension system).

Method

Head model

The FE meshes of the head–brain–neck complex were developed using a commercially available database (Materialise, Leuven, Belgium). The FE models were constructed using a commercially available software ABAQUS (version 6.9, Dassault Systèmes, Walthamn, MA, USA). The surface scans of the skin (Figure 1(a)), skull (Figure 1(b)), and brain (Figure 1(c)) were applied to generate the FE meshes in this study. These scans were obtained by computed tomography (CT) scans of living subjects and the dimensions of these surface meshes represent approximately the 50th percentile of Caucasian males.

The head–brain–neck complex consisted of scalp, skin tissues, skull, cervical vertebrae (C1, C2, and C3), discs, brain, medulla, CSF, and spinal cord (Figure 1(d)). The brain tissues included the cerebrum, cerebellum, and a part of the brainstem (midbrain and pons) (Figure 1(a)). The spinal cord included the surrounding pia mater. The CSF was considered to cover the entire external surface of the brain, medulla, and the spinal cord (Figure 1(d)). The discs contained both annulus fibrosus and nucleus pulposus. Within each of these components (i.e. brain, medulla, CSF, spinal cord, and discs), the material was considered homogeneous. The connections between the tissues were assumed to be perfect bond, without relative sliding during deformation. The CSF had a thickness of 1.3 mm and was constructed using membrane elements (element: M3D4), whereas all other components were constructed using three-dimensional (3D) continuous elements (element: C3D4). The entire head model contains 34,970 elements and 72,185 degrees of freedom (DOFs).

Helmet and falling object models—The helmet model consisted of a shell and a suspension system. The shell geometry was obtained by scanning a representative, commercially available construction helmet (Model V-Gard; MSA Safety Inc., Pittsburgh, PA, USA). The geometry of the suspension system was constructed using commercially available software (Autodesk, Inc., San Rafael, CA, USA). The 3D geometries of the shell and suspension were then imported into ABAQUS to generate FE meshes (Figure 2(a) and (b)). The model of the helmet shell was constructed using shell elements (element: S4), whereas that of the suspension system was generated using 3D continuous elements (element: C3D8R). The suspension system was constrained to the helmet shell at four plug locations. The head–brain–helmet complex model is shown in Figure 2(c) and (d). The falling object was cylindrical (diameter: 28.5 mm, length: 100 mm) and was modeled using 3D continuous elements (element: C3D8R).

Material properties

Mechanical properties of the hard and soft tissues—The scalp, skull bone, cervical discs, and vertebral bone were considered to be linearly elastic. The elastic modulus and Poisson's ratio of the scalp were assumed based on the experimental data by Galford and McElhaney[21] and the viscous deformation was neglected. The material properties of the cervical discs were based on the test data by Schmidt et al.;[22] the effects of the interstitial fluid were neglected. The same elastic material properties were applied to the skull and

vertebral bone.[23] The CSF was considered as a weak, elastic, and nearly incompressible medium.[8]

The skin, brain, medulla, and spinal cord were considered to be hyperelastic and viscoelastic. The finite deformation formulation was used in describing the constitutive models due to large tissue deformations. The hyperelastic properties of the skin, brain, brainstem, and spinal cord tissues were modeled using a generalized Mooney–Rivlin equation, which is governed by a strain energy potential

$$U = C_{10}(\bar{I}_1 - 3) + C_{01}(\bar{I}_2 - 3) + C_{11}(\bar{I}_1 - 3)(\bar{I}_2 - 3) + \frac{1}{D_1}(J - 1)^2 \tag{1}$$

where $\bar{I}_1$, $\bar{I}_2$, and J are the first and second deviatoric strain invariants and the volumetric ratio, respectively; C_{10}, C_{01}, C_{11}, and D_1 are the material parameters.

The elastic stress in the tissues (Cauchy stress), σ_{ij}^0, is related to the strain energy density by

$$\sigma_{ij}^0 = \frac{2}{J} F_{ir} \frac{\partial U}{\partial C_{rs}} F_{sj}; \quad i, j = 1, 2, 3 \tag{2}$$

where F_{ij} and C_{ij} are the tensors of the deformation gradient and the right Cauchy–Green deformation, respectively.

Neglecting the volumetric viscoelastic deformation, the shear viscoelastic properties of the tissues were determined by three-term Prony series

$$g(t) = 1 - \sum_{i=1}^{2} g_i \left(1 - e^{-\frac{t}{\tau_i}}\right) \tag{3}$$

where g_i and τ_i ($i = 1, 2, 3$) are shear and relaxation time parameters, respectively.

The total tissue stress (Cauchy stress), $\sigma_{ij}(t)$, was composed of an elastic stress [$\sigma_{ij}^0(t)$], representing instantaneous tissue response, and a viscous stress ($\sigma_{ij}^v(t)$), representing delayed tissue response

$$\sigma_{ij}(t) = \sigma_{ij}^0(t) + \int_0^t \dot{g}(\tau) S_{ij}^0(t - \tau) d\tau; \quad i, j = 1, 2, 3 \tag{4}$$

where S_{ij}^0 is the elastic stress deviator, which is defined as $S_{ij}^0 = \sigma_{ij}^0 - (1/3)\sigma_{kk}^0 \delta_{ij}$ with δ_{ij} being the Kronecker delta.

The nonlinear elastic properties of the skin were determined using the in vivo test data of human skin by Hendriks et al.;[24,25] the viscoelastic properties of the skin were determined based on Wu et al.[26] The nonlinear elastic and viscoelastic parameters of the brain were determined based on the dynamic test data by Rashid et al.[27] The viscous properties of the medulla were assumed to be identical to those of the brain, whereas the nonlinear elastic parameters were determined based on the data by Arbogast and Margulies.[28] The nonlinear elastic and viscoelastic properties of the spinal cord were determined based on the data by Bilston and Thibault[29] and Mazuchowski and Thibault.[30] All material parameters of the hard and soft tissues are listed in Table 1.

Mechanical properties of the helmet and falling object—The helmet shell was considered to be made of typical acrylonitrile butadiene styrene (ABS) plastic.[31] The suspension's top belt side ring was considered to be of high strength polymers. The front cushion of the suspension system was of soft foam material. The falling cylinder was considered to be made of steel ($E = 210\,GPa$, $\nu = 0.3$, and specific density = 7.8) and had a mass of 2 kg. All these materials were considered to be linearly elastic and the material parameters are listed in Table 1.

Simulation procedures

Two series of numerical simulations were performed in this study. The first series of the numerical tests was to calibrate and verify the head–brain–neck model using the experimental data by Nahum et al.[32] The second series of numerical tests was to investigate the responses of the head–brain to the impact of an object on top of the helmet. Of special interest was an evaluation of the effects of the neck and body mass on the responses of the head–brain during the impact.

Calibration and verification of the head–brain model—The numerical test was to mimic the set-up of the cadaveric tests by Nahum et al.,[32] as illustrated in Figure 3. The head model was tilted forward, such that the Frankfort anatomical plane was inclined by 45° to the horizontal plane. The object was impacted at the head at the frontal bone and in the mid-sagittal plane. A point mass of 10 kg was connected to the vertebral bone at the neck, simulating the portion of the body mass participating in the dynamic responses. The impacting object was cylindrical and had a diameter of 50 mm and a height of 30 mm. The impact force, which was measured in the experiment,[32] was applied uniformly at the back of the cylindrical impact pad (Figure 3). The simulations were conducted in a force-controlled manner; no boundary conditions were applied on the model. In the impact tests by Nahum et al.,[32] the intracranial pressures were measured at the frontal, parietal, occipital, and posterior fossa locations of the brain, which will be used to calibrate the current FE model. The pressures in the brain tissues at these four locations as well as the head accelerations calculated using the proposed model will be compared with those measured experimentally.

Simulations of top impact on the helmet—The helmet was fitted onto the head due to its own weight. Initially, the cylinder was at a height of 3.27 m above the helmet top. For $t >$ 0, the cylinder was released and fell due to gravity; it reached a speed of 8 m/s just before impacting with the helmet (Figure 4). The falling object made the contact with the helmet shell at the center. The simulations were performed using an implicit dynamic procedure.

In order to investigate the effects of the neck and body mass on the head–brain responses during the impact, three numerical tests with different neck boundary conditions were performed. In impact simulation A (Figure 4(a)), no constraint boundary conditions were applied and the effects of the neck on head–brain responses became negligible. In impact simulation B (Figure 4(b)), a point mass of 10 kg, which represented the effects of the body, was connected to the vertebral bone at the neck, whereas no boundary condition was applied. In impact simulation C (Figure 4(c)), the neck was constrained in all three directions, whereas the soft tissues (spinal cord and skin tissues) at the neck were constrained only in the vertical direction. Consequently, the soft tissues at the neck remained in a flat plane, while its cross-sectional shape could vary during the impact deformation.

None of simulations A, B, or C represents true physiological conditions. In simulation A, the effects of the neck were completely ignored. The boundary at the neck was over-constrained in simulation C, whereas it was under-constrained in simulation B. The boundary at the neck for the real physiological conditions may be between those for simulations B and C. Therefore, the solutions obtained from simulations B and C may represent the upper and lower bounds of the true solution. If the difference between the solutions of simulations B and C is small, the true solution can be reasonably estimated using the average of those for simulations B and C.

Head injury criteria—Severity of the impact for each of the numerical tests has been evaluated using the head injury criteria (HIC),[33,34] which is defined by

$$HIC = \text{Max} \left((t_1 - t_0) \left[\frac{1}{t_1 - t_0} \int_{t_0}^{t_1} a(\tau) d\tau \right]^{2.5} \right) \tag{5}$$

where a is the resultant head acceleration measured in g and t_0 and t_1 are the beginning and end of the time interval, respectively. The time interval used for the HIC calculation is required to be less than 36 ms. HIC score was calculated by an iterative search to find the time interval (t_0, t_1), at which the HIC score is maximized.

An HIC score of 1000 is considered as the "safe" limit for human tolerance, based on the studies of sports surfacing and shock attenuation performance.[35] The relationship between HIC scores and the probability of head injuries has been established and widely used in the automotive industry to estimate the injury risk.[36,37] An impact with an HIC score of 1000 will represent less than 3% chance of getting a critical or fatal head injury.[37]

Results

Model calibration and verification

The responses of the head and brain during impact that were predicted using the current head–brain FE model (Figure 3) were compared with those measured in Nahum et al.'s[32] experiments (Test #37 in Nahum et al.[32]). The calculated time histories of the contact force between the impact cylindrical pad and the head and the corresponding head accelerations are compared with the experimental data, as shown in Figure 5(a) and (b). The contact force calculated via the FE model is consistent with the test data, except for the first 0.5 ms, where the curve for the test data is smooth, whereas the calculated curve shows some jitters. This is due to the process of the establishment of the initial contact between the impacting object and front of the head.

The comparisons of the calculated and measured intracranial pressures[32] during the impact at frontal, posterior fossa, parietal, and occipital positions are shown in Figure 6(a)–(d), respectively. There are two measurements for the occipital pressures[32] and both are shown in Figure 6(d). In the FE modeling, the mechanical pressures in the brain tissues were considered as the intracranial pressures.

Responses of the head and brain to impact when wearing a helmet

The time histories of the contact force between the scalp and the helmet suspension during the impacts with helmet are shown in Figure 7(a). The peak contact force was found around 2.85 ms and to be 6119.9, 7328.7, and 7345.8 N for impact simulations A, B, and C, respectively. Correspondingly, the time histories of the head acceleration magnitude during the impacts are shown in Figure 7(b). The head accelerations reach maximum around 3.65 ms and peaked at 1350.9, 1244.9, and 1188.1m/s^2 for impact simulations A, B, and C, respectively. The head accelerations are predominantly in the vertical direction.

The time histories of the brain pressures at the parietal and posterior fossa locations are shown in Figure 7(c) and (d), respectively. The maximal and the minimal brain pressures during the impact were found at the parietal and posterior fossa regions, respectively, and around 3.65 ms, when the accelerations reached the maximum. The distributions of the brain pressures at $t = 3.65$ms, when the extreme values occurred, for impact simulations A, B, and C are shown in Figure 8(a)–(c), respectively.

Based on the time histories of the head accelerations (Figures 5(b) and 7(b)), HIC scores for the calibration and impact simulations were calculated and are shown in Table 2. The time intervals (t_0 and t_1) used to calculate the HIC score, together with the maximal accelerations and impact forces for the numerical tests, are also shown in Table 2.

Discussion and conclusion

For biomedical engineering applications, it is difficult to precisely account for the effects of the neck and body mass on the dynamic responses of the head–brain in FE modeling,[38] because FE modeling usually does not include the entire human body. In this study, we have established reasonable upper and lower bounds of the precise solutions for this particular

problem. The stiffness of the neck for a real person should be higher than that for model B (Figure 4(b)), whereas lower than that for model C (Figure 4(c)). Our analysis indicated that the first peaks of the acceleration and impact force of the head obtained using the model B differ by less than 1% from those obtained using model C. Therefore, a good estimation for the precise solution is obtained by an average of the solutions obtained using models B and C (Table 2).

Using the proposed approach, the estimated HIC score, peak acceleration, and peak contact force for the impact with helmet are calculated to be 213.8 s, 1206.5m/s^2, and 7337.3 N, respectively (Table 2). If the effects of the neck and body mass are neglected (i.e. model A), HIC score and the peak head acceleration are overestimated by 33% and 12%, respectively, whereas the peak impact force is underestimated by 17%. The effects of the neck and body mass on the second peaks of the acceleration and impact force are more dramatic (Figure 7); however, these parameters are not important for the injury criterion.

Our analysis indicated that exclusion of the effects of the neck and body mass not only caused an overestimation by 6%–12% of the peak brain pressures at the parietal and posterior fossa locations (Figure 7), but also varied the patterns of the time histories of the brain pressures. For the simulations with the neck effects (models B and C), the parietal pressure tends to reverse from positive to negative and reaches a bottom around 7.5 ms; the posterior fossa pressure tends to reverse from negative to positive and reaches an apex around the same time. However, when the neck effects are neglected (model A), the brain pressures did not reverse and tended to monotonically reduce to zero with an increase in time.

The comparison of the model prediction with the tests in the calibrations demonstrated good agreement between the predicted brain pressures and the experimental measurements at all four locations (Figures 5 and 6) and thus confirmed the reliability of the proposed head–brain model. The maximal head acceleration and HIC score are predicted to be 1905m/s^2 and 775 s, compared to the corresponding experimental data of 2000m/s^2 and 744 s, respectively. The difference between the calculated and the experimentally measured parameters values is within 5%.

The CSF plays an important role in absorbing the dynamic energy transmitted to the brain during the impact. The effects of the CSF are clearly demonstrated in the predicted brain pressures. When the CSF was included, the predicted frontal pressure goes to the peak and then reduces to zero monotonically (Figure 6(a)); however, when the CSF was not included, the frontal pressure would go to the negative region after reaching the peak and gradually reduce to zero after several cycles.[17,32] Nevertheless, the CSF seems to have little effects on the first peak magnitudes of the predicted brain pressures.[17]

The HIC score for the top impact with helmet was estimated to be 214 (Table 2) using the proposed model, and it is comparable to the HIC(d) (226) (normalized HIC) whereas it is substantially greater than the raw HIC score (79) obtained by a previous study.[17] These differences may be caused by the difference in the modeling of the helmet suspension system. The material and structural variations of the suspension system will substantially

vary the performance and characteristics of a helmet. In this helmet model, representative material and structural properties have been assumed. For practical applications, the helmet suspension systems need to be more precisely modeled, real structural and material properties should be applied, and the models need to be calibrated with experimental data.

In this study, the cervical discs were considered as isotropic and linearly elastic. The cervical discs are complex in mechanical properties; they are not only biphasic, composed of a solid and a fluid phase, but also anisotropic due to the reinforce effects of the distributed collagen fibers within the tissues.[39] If the major concern is the injury mechanism of the cervical discs, it is necessary to know the loading share between the fluid and solid phases; in that case, the interstitial fluid and collagen become non-negligible effects. However, in this study, we need to only know the mechanical response of the cervical discs when subjected to shock load; we are not interested in the detailed stress/strain distributions within the tissues. In this scenario, it is reasonable to simplify the cervical discs as isotropic and linearly elastic.

Typical falling objects in construction site are small and have a mass less than 2 kg, such as hand tools, bricks, bolts. The mass and dimension of the falling object simulated in this study are representatives for real situations. In the simulations, we selected an impact velocity of 8 m/s for the falling object, which is approximately correspondent to a fall height of 5 m, assuming a worker has a height of 1.8 m. This height is typical at construction sites of residential buildings in the United States. The purpose of this study is to develop a model; once the model is validated, it can be applied to analyze or numerically reconstruct the accidents in construction sites.

In summary, we proposed an approach to estimate the effects of the neck and body mass on the dynamic responses of the head–brain during impacts. Using the proposed approach, we have calculated the responses of the head–brain during a top impact when wearing a construction helmet. The proposed modeling approach would make it possible to improve the helmet design on a biomechanical basis.

Acknowledgments

References

1. Faul, M., Xu, L., Wald, M., et al. Technical Report. Centers for Disease Control and Prevention; Atlanta, GA: Mar. 2010 Traumatic brain injury in the United States: emergency department visits, hospitalizations and deaths 2002–2006.

2. Tiesman HM, Konda S, Bell JL. The epidemiology of fatal occupational traumatic brain injury in the U. S Am J Prev Med. 2011; 41(1):61–67. [PubMed: 21665064]

3. Voo K, Kumaresan S, Pintar FA, et al. Finite-element models of the human head. Med Biol Eng Comput. 1996; 34(5):375–381. [PubMed: 8945864]

4. Hardy CH, Marcal PV. Elastic analysis of a skull. J Appl Mech: T ASME. 1973; 40:838–842.

5. Kenner VH, Goldsmith W. Dynamic loading of a fluid-filled spherical shell. Int J Mech Sci. 1972; 14(9):557–568.

6. Willinger R, Kang HS, Diaw B. Three-dimensional human head finite-element model validation against two experimental impacts. Ann Biomed Eng. 1999; 27(3):403–410. [PubMed: 10374732]

7. Kleiven S, Hardy WN. Correlation of an FE model of the human head with local brain motion— consequences for injury prediction. Stapp Car Crash J. 2002; 46:123–144. [PubMed: 17096222]

8. Yan W, Pangestu OD. A modified human head model for the study of impact head injury. Comput Methods Biomech Biomed Engin. 2011; 14(12):1049–1057. [PubMed: 21264785]

9. Patton DA, McIntosh AS, Kleiven S. The biomechanical determinants of concussion: finite element simulations to investigate tissue-level predictors of injury during sporting impacts to the unprotected head. J Appl Biomech. 2015; 31(4):264–268. [PubMed: 25781376]

10. Tse KM, Tan LB, Lee SJ, et al. Development and validation of two subject-specific finite element models of human head against three cadaveric experiments. Int J Numer Method Biomed Eng. 2014; 30(3):397–415. [PubMed: 24574171]

11. Tse KM, Tan LB, Lee SJ, et al. Investigation of the relationship between facial injuries and traumatic brain injuries using a realistic subject-specific finite element head model. Accid Anal Prev. 2015; 79:13–32. [PubMed: 25795050]

12. Ruan JS, Khalil T, King AI. Dynamic response of the human head to impact by three-dimensional finite element analysis. J Biomech Eng. 1994; 116(1):44–50. [PubMed: 8189713]

13. Willinger R, Taleb L, Kopp CM. Modal and temporal analysis of head mathematical models. J Neurotrauma. 1995; 12(4):743–754. [PubMed: 8683626]

14. Afshari A, Rajaari SM. Finite element simulations investigating the role of the helmet in reducing head injuries. Int J Simulat Model. 2008; 7(1):42–51.

15. Teng T, Liang C, Nguyen V. Development and validation of finite element model of helmet impact test. Proc IMechE, Part L: J Materials Design and Applications. 2012; 227:82–88.

16. Yang J, Dai J. Simulation-based assessment of rear effect to ballistic helmet impact. Comput Aided Des Appl. 2010; 7(1):59–73.

17. Long J, Yang J, Lei Z, et al. Simulation-based assessment for construction helmets. Comput Methods Biomech Biomed Engin. 2015; 18(1):24–37. [PubMed: 23495784]

18. Gilchrist A, Mills NJ. Construction site workers helmets. J Occup Accid. 1987; 9:199–211.

19. Mills N, Gilchrist A. Industrial helmet performance in impacts. Safety Sci. 1993; 16:221–238.

20. Suderman BL, Hoover RW, Ching RP, et al. The effect of hardhats on head and neck response to vertical impacts from large construction objects. Accid Anal Prev. 2014; 73:116–124. [PubMed: 25215927]

21. Galford JE, McElhaney JH. A viscoelastic study of scalp, brain, and dura. J Biomech. 1970; 3(2): 211–221. [PubMed: 5521539]

22. Schmidt H, Haussler K, Wilke HJ, et al. Structural behavior of human lumbar intervertebral disc under direct shear. J Appl Biomater Funct Mater. 2015; 13(1):66–71. [PubMed: 24744233]

23. Yamada, H., Evans, FG. Strength of biological materials. Baltimore, MD: Lippincott Williams & Wilkins; 1970.

24. Hendriks FM, Brokken D, Van Eemeren JT, et al. A numerical-experimental method to characterize the nonlinear mechanical behaviour of human skin. Skin Res Technol. 2003; 9(3): 274–283. [PubMed: 12877691]

25. Hendriks FM, Brokken D, Oomens CW, et al. Influence of hydration and experimental length scale on the mechanical response of human skin in vivo, using optical coherence tomography. Skin Res Technol. 2004; 10(4):231–241. [PubMed: 15479446]

26. Wu JZ, Dong RG, Smutz WP, et al. Effects of preconditioning on the elastic behavior of skin under compressive loading. J Mech Med Biol. 2003; 3(3–4):275–283.

27. Rashid B, Destrade M, Gilchrist MD. Mechanical characterization of brain tissue in simple shear at dynamic strain rates. J Mech Behav Biomed Mater. 2013; 28:71–85. [PubMed: 23973615]

28. Arbogast KB, Margulies SS. Material characterization of the brainstem from oscillatory shear tests. J Biomech. 1998; 31(9):801–807. [PubMed: 9802780]

29. Bilston L, Thibault L. The mechanical properties of the human cervical spinal cord in vitro. Ann Biomed Eng. 1996; 24:67–74. [PubMed: 8669719]

30. Mazuchowski, E., Thibault, L. Biomechanical properties of the human spinal cord and pia mater. 2003. http://www.tulane.edu/sbc2003/pdfdocs/1205.PDF

31. Kwon, H., Choi1, W., Choi, J., et al. Mechanical behavior analyses of plastics under environmental changes. Proceedings of the 18th international conference on composite materials; Jeju Island, South Korea. 21–26 August 2011;

32. Nahum, A., Smith, R., Ward, C. Intracranial pressure dynamics during head impact. Proceedings of the 21st Stapp Car Crash Conference; Warrendale, PA, USA. 19–21 October 1977; p. 339-366.

33. Eppinger, R. Chapter 5: A prospective view of head injury research. In: Bandak, FA.Eppinger, RH., Ommaya, AK., editors. Traumatic brain injury: bioscience and mechanics. Larchmont, NY: Mary Ann Liebert, Inc; 1996. p. 39-45.

34. Patel, A., Goswami, T. Comparison of intracranial pressure by lateral and frontal impacts— validation of computational model. In: Goswami, T., editor. Injury and skeletal biomechanics. Vol. Chapter 6. Rijeka: InTech; 2012. p. 95-114.

35. Shorten, M., Himmelsbach, J. Sports surfaces and the risk of traumatic brain injury. Calgary, AB, Canada: University of Calgary; 2003.

36. NHTSA. Technical Report. National Highway Traffic Safety Administration; Washington, DC: 1997. Head impact protection. 49 CFR Parts 571. [Docket No. 92–28; Notice 8] http://www.nhtsa.gov/cars/rules/rulings/headprot/pubnprm.html

37. Prasad, P., Mertz, H. Technical Report. Society of Automotive Engineers; Warrendale, PA: Jun. 1985 The position of the United States delegation to the ISO working group on the use of HIC in the automotive environment.

38. Kimpara H, Iwamoto M, Watanabe I, et al. Effect of assumed stiffness and mass density on the impact response of the human chest using a three-dimensional FE model of the human body. J Biomech Eng. 2006; 128(5):772–776. [PubMed: 16995765]

39. Wu JZ, Herzog W, Federico S. Finite element modeling of finite deformable, biphasic biological tissues with transversely isotropic statistically distributed fibers: toward a practical solution. Z Angew Math Phys. 2016; 67:26. [PubMed: 27330228]
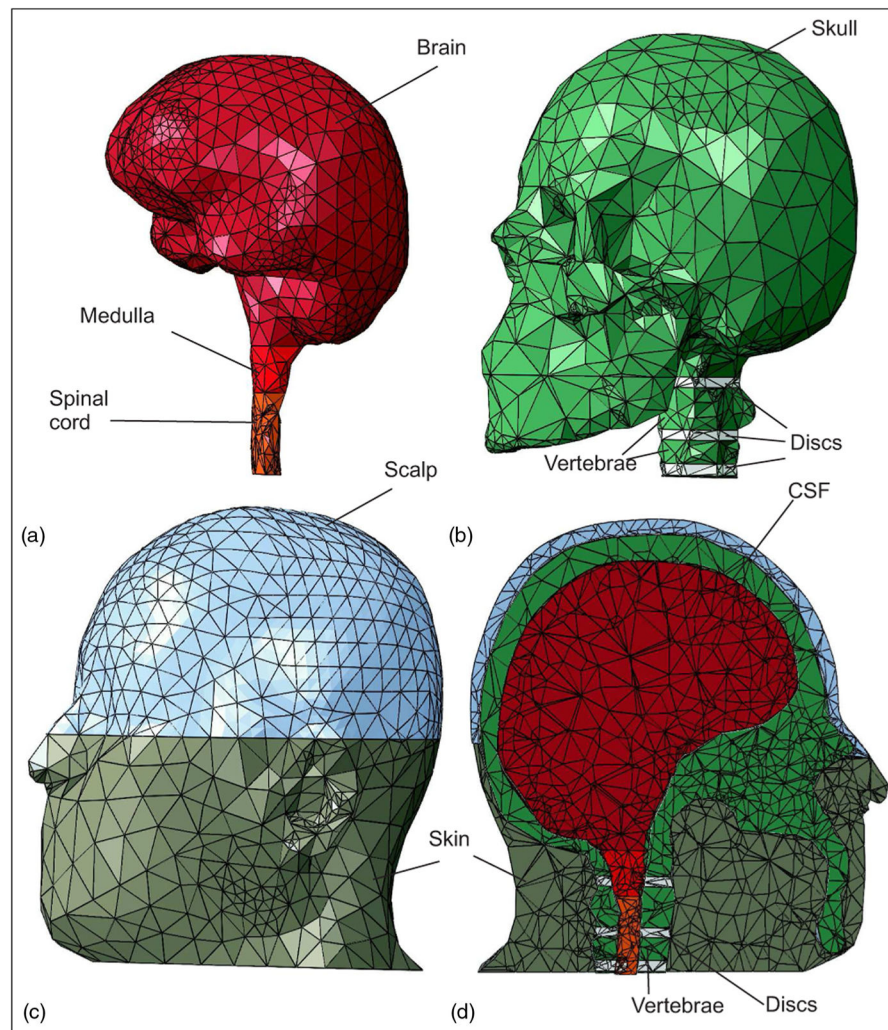
Figure 1.
FE model of the human head: (a) brain, medulla, and spinal cord; (b) skull, vertebrae, and discs; (c) scalp and skin tissues; and (d) cross-sectional view of the entire head model.
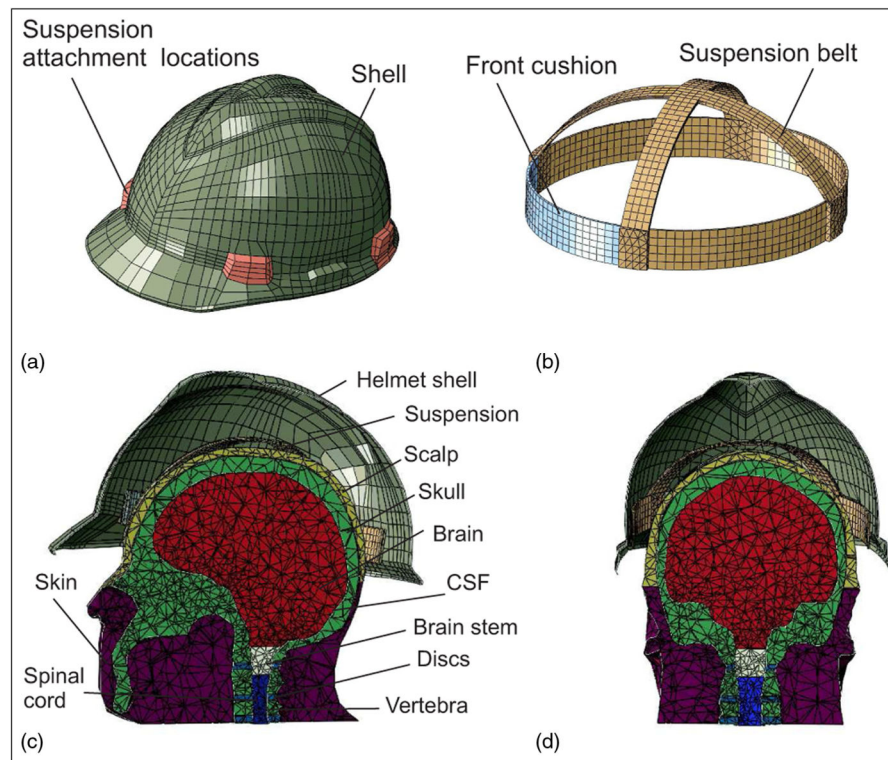
Figure 2.
FE model of the head–helmet complex: (a) helmet shell, (b) helmet suspension system, (c) cross-sectional view in the sagittal plane, and (d) cross-sectional view in the coronal plane.
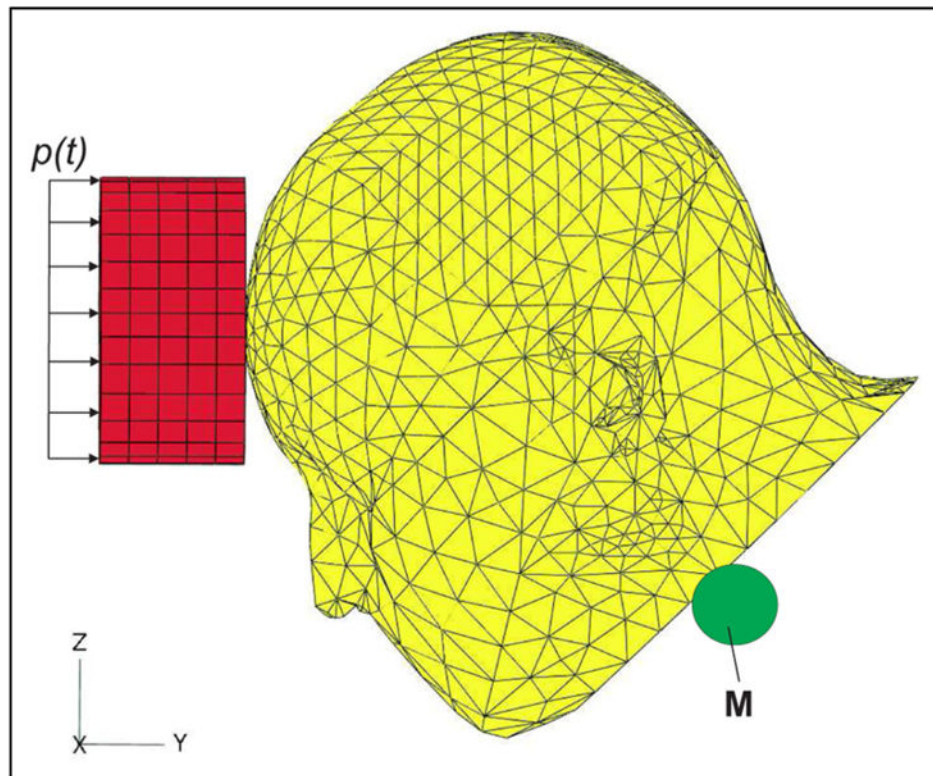
Figure 3.
Set-up of the numerical calibration test. A concentrated mass of 10 kg was attached to the neck bone; a distributed load was applied on the back of the cylindrical impact pad; no boundary constraints were applied to the model during the impact.
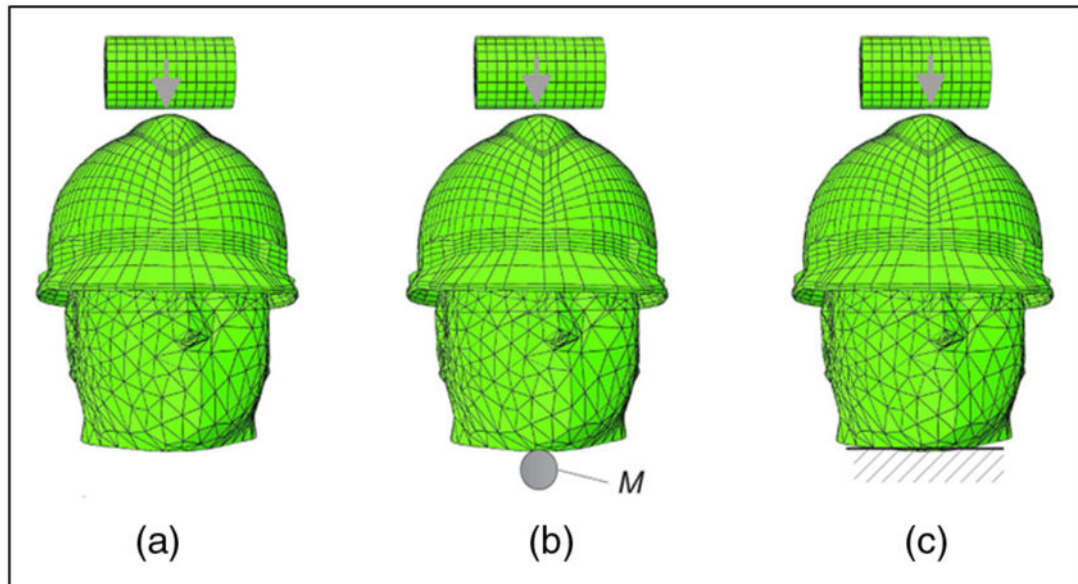
Figure 4.
Set-up of the helmet impact simulations with different boundary conditions at the neck: (a) model for impact simulation A: was free, (b) model for impact simulation B: a concentrated mass of 10 kg was attached to the neck bone; no boundary constraints were applied, and (c) model for impact simulation C: the neck bone was fixed in all three directions. A cylindrical object fell from a height of $h = 3.27$m and impacted with the helmet at a speed of 8 m/s.
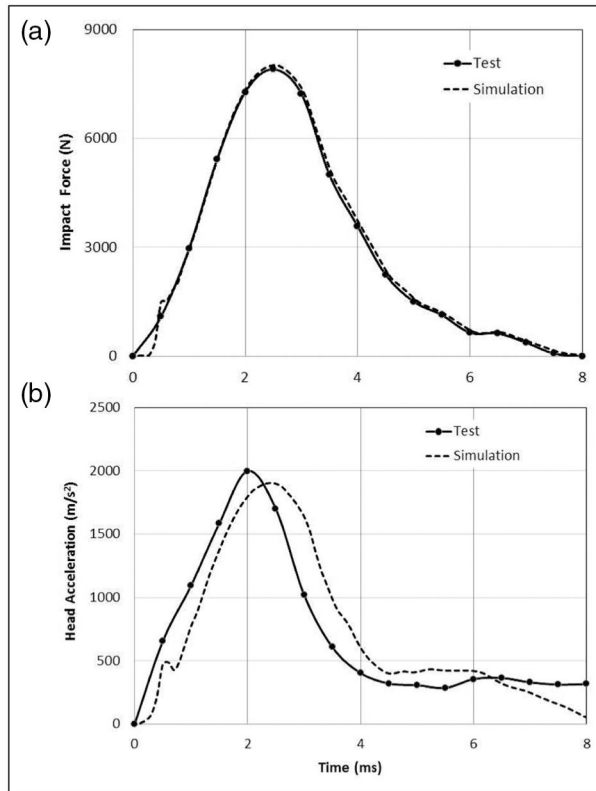
Figure 5.
(a) The comparison of the impact force and (b) head acceleration calculated using the FE model with those measured in the experiment.[32]
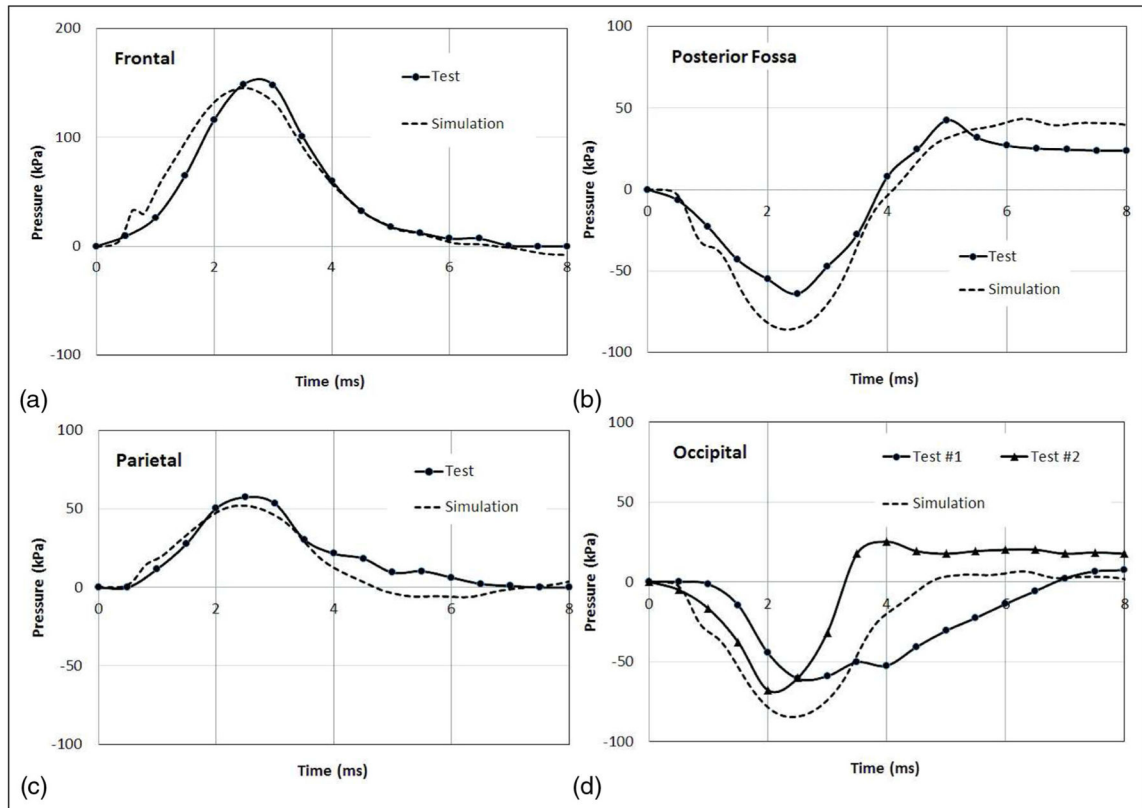
Figure 6.
The comparison of the brain pressures at the (a) frontal, (b) posterior fossa, (c) parietal, and (d) occipital locations calculated using the FE model with those measured in the experiment.[32]
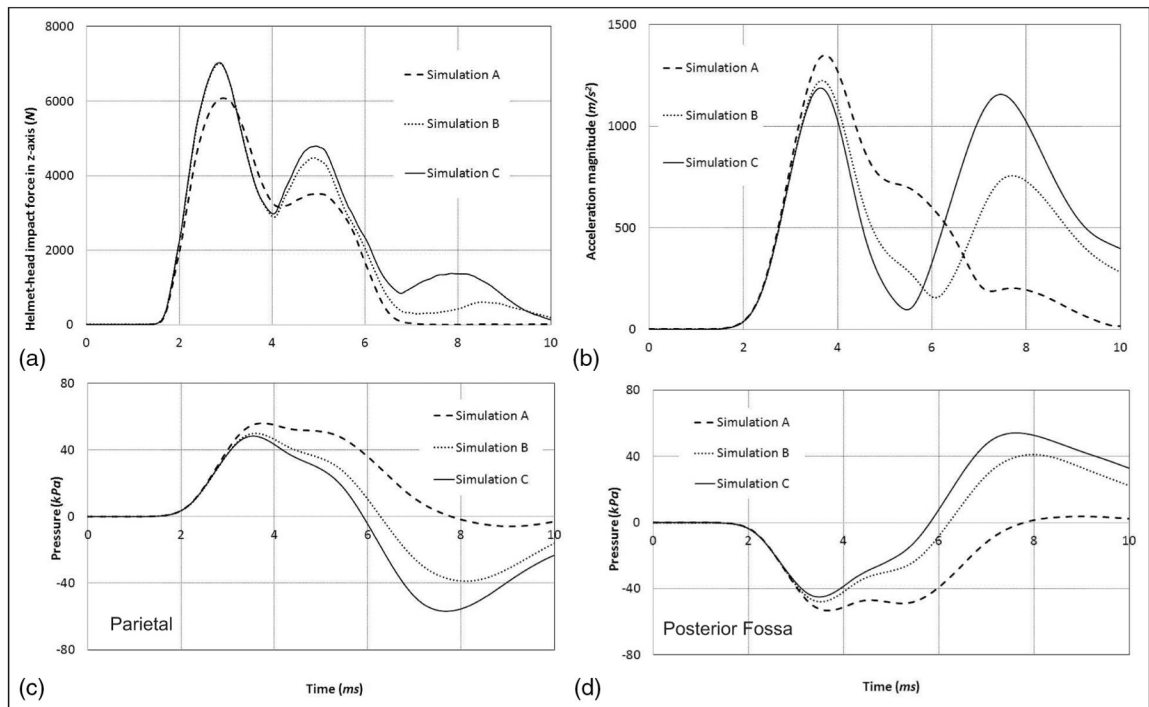
Figure 7.
The time histories of the impact force, acceleration, and brain pressure for impact simulations A, B, and C: (a) vertical impact force, (b) acceleration magnitude, (c) parietal pressure, and (d) posterior fossa pressure.
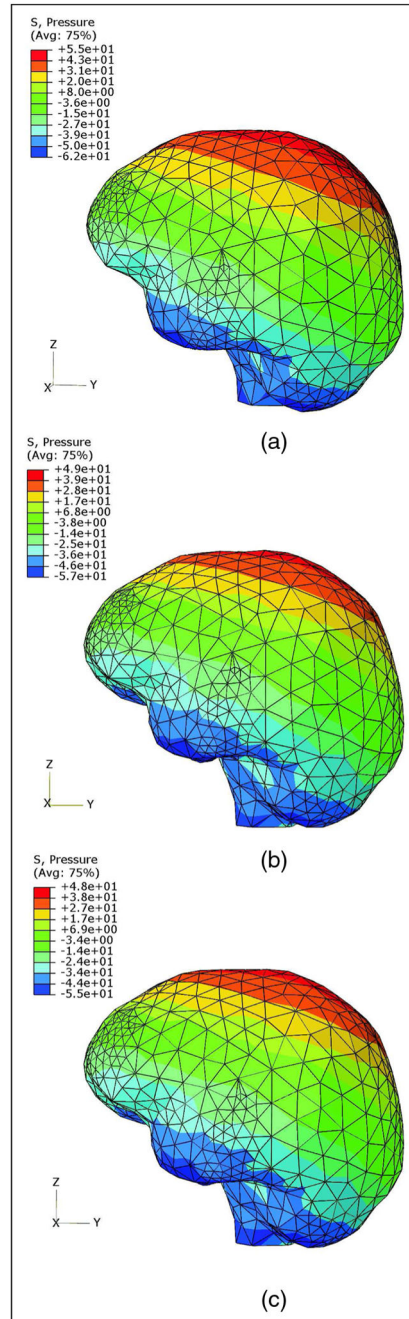
Figure 8.

The distributions of the brain pressures at $t = 3.65$ ms: (a–c) the results obtained in the impact simulations A, B, and C, respectively. The maximal and minimal pressure values occurred in the parietal and posterior fossa regions, respectively.

Table 1

The material parameters of the hard and soft tissues and the helmet components used in the FE modeling.

Material	Specific density	Elastic property	Viscous property	Damping (β)	References
Brain	1.04	$C_{10} = C_{01} = 0.263$ kPa	$g_1 = 0.59, g_2 = 0.39, g_3 = 0.0009$; $\tau_1 = 0.00059$ s, $\tau_2 = 0.0014$ s, $\tau_3 = 0.01$ s	0.0001	Rashid et al.[27]
Medulla	1.04	$C_{20} = C_{02} = 0.491$ kPa, $D_1 = 0.0019$ kPa^{-1}; $C_{10} = 0.75$ kPa, $D_1 = 0.001$ kPa^{-1}	$g_1 = 0.59, g_2 = 0.39, g_3 = 0.0009$; $\tau_1 = 0.00059$ s, $\tau_2 = 0.0014$ s, $\tau_3 = 0.01$ s	0.001	Arbogast and Margulies[28]
Spinal cord	1.04	$C_{10} = 14.8$ kPa, $D_1 = 0.001$ kPa^{-1}	$g_1 = 0.52, g_2 = 0.3057$; $\tau_1 = 0.0264$ s, $\tau_2 = 0.011$ s	0.001	Mazuchowski and Thibault[30]; Bilston and Thibault[29]
Skin	1.01	$C_{10} = 9.4, C_{11} = 82$ kPa; $D_1 = 0.01$ kPa^{-1}	$g_1 = 0.295, g_2 = 0.349$; $\tau_1 = 0.373$ s, $\tau_2 = 5.592$ s	0.01	Hendriks et al.[24,25]; Wu et al.[26]
Scalp	1.2	$E = 16.7$ MPa, $\nu = 0.42$		0.001	Galford and McElhaney[21]
Discs	1.2	$E = 4.8$ MPa, $\nu = 0.22$		0.001	Schmidt et al.[22]
Bone (skull/vertebrae)	2.09	$E = 6.0$ GPa, $\nu = 0.19$		0.001	Yamada and Evans[23]
CSF	1.04	$E = 150$ MPa, $\nu = 0.499$		0.001	Yan and Pangestu[8]
Helmet shell	1.2	$E = 3$ GPa, $\nu = 0.33$		0.001	Kwon et al.[31]
suspension belt	1.2	$E = 2$ GPa, $\nu = 0.3$		0.001	
front cushion	1.2	$E = 250$ MPa, $\nu = 0.3$		0.001	
Falling object (steel)	7.8	$E = 210$ GPa, $\nu = 0.30$		0.001	

CSF: cerebrospinal fluid.

Table 2

The HIC (head injury criteria) and the maximal head acceleration magnitude and impact force obtained in the simulations. .

	Att. mass (kg)	B.C.	t_0 (ms)	t_1 (ms)	HIC (s)	A_{max} (m/s^2)	F_{max} (N)
Calibration	10	Free	1.1	3.5	771.8	1905.3	8000.0
Impact A	0	Free	2.9	6.2	284.5	1350.9	6119.9
Impact B	10	Free	2.6	9.4	198.7	1224.9	7328.7
Impact C	10	Fix	6.2	9.1	228.9	1188.1	7345.8
Estimation	–	–	4.4	9.2	213.8	1206.5	7337.3

HIC: head injury criteria. Att. mass: attached mass. B.C.: boundary condition. A, B, and C represent the impact simulations A, B, and C with helmet, as illustrated in Figure 3(a)–(c), respectively. t_0 and t_1 represent the start and end of the time interval, respectively, during which the HIC was calculated.